THE ASTROPHYSICAL JOURNAL, 559:296–303, 2001 September 20
© 2001. The American Astronomical Society. All rights reserved. Printed in U.S.A.

COSMIC-RAY ELECTRONS AND POSITRONS FROM 1 TO 100 GeV: MEASUREMENTS WITH HEAT AND THEIR INTERPRETATION

M. A. DUVERNOIS,[1,2] S. W. BARWICK,[3] J. J. BEATTY,[1] A. BHATTACHARYYA,[4] C. R. BOWER,[4] C. J. CHAPUT,[5] S. COUTU,[1] G. A. DE NOLFO,[1,6] D. M. LOWDER,[7] S. MCKEE,[5] D. MÜLLER,[8] J. A. MUSSER,[4] S. L. NUTTER,[1,9] E. SCHNEIDER,[3] S. P. SWORDY,[8] G. TARLÉ,[5] A. D. TOMASCH,[5] AND E. TORBET[8,10]

Received 2000 October 25; accepted 2001 May 17

ABSTRACT

Measurements of the energy spectra of negative electrons and positrons have been performed with the High-Energy Antimatter Telescope (HEAT) in two balloon flights—1994 May from Fort Sumner, NM, and 1995 August from Lynn Lake, Manitoba. We present the combined data set from these two flights, covering the energy range 1-100 GeV. We compare our data with results from other groups and discuss the data in the context of diffusive propagation models. There is some evidence that primary electrons above 10 GeV and cosmic-ray nuclei exhibit the same energy spectrum at the source, but that the source spectrum becomes harder at lower energy. Within the experimental uncertainties, the intensity of positrons is consistent with a purely secondary origin, due to nuclear interactions in interstellar space.

Subject headings: cosmic rays — elementary particles — ISM: abundances

On-line material: color figures

1. INTRODUCTION

The electron component in the cosmic radiation consists of negative electrons and positrons. A number of measurements of their energy spectrum (the combined spectrum, e^+ and e^-) up to about 2 TeV (e.g., Prince 1979; Nishimura et al. 1980; Golden et al. 1984; Tang 1984; Kobayashi et al. 1999) have shown that the electron intensity, about 1% of the proton intensity at 10 GeV, decreases more rapidly with energy than that of cosmic-ray nuclei. While the existing data exhibit sizeable statistical and systematic uncertainties, it is clear that the power-law index of the electron spectrum above 10 GeV is larger than 3.0, in contrast to the proton index of $\sim$2.7. Early measurements capable of separating electrons and positrons have shown that the positron fraction $[e^+/(e^+ + e^-)]$ is around 10% in the 1–10 GeV region (Fanselow et al. 1969; Buffington, Orth, & Smoot 1975). Subsequent work indicated an unexpected increase in the positron fraction above 10 GeV (Müller & Tang 1987; Golden et al. 1987), which, however, was not confirmed in more recent observations (Barwick et al. 1995; Barbiellini et al. 1996; Barwick et al. 1997a).

[1] Departments of Physics and of Astronomy and Astrophysics, 104 Davey Laboratory, Pennsylvania State University, University Park, PA 16802.

[2] Present address: School of Physics and Astronomy, University of Minnesota, 116 Church Street SE, Minneapolis, MN 55455.

[3] Department of Physics, University of California at Irvine, Irvine, CA 92717.

[4] Department of Physics, Swain Hall West, Indiana University, Bloomington, IN 47405.

[5] Department of Physics, Randall Laboratory, 500 E. University, University of Michigan, Ann Arbor, MI 48109.

[6] Present address: Space Research Laboratory, M/S 220-47, California Institute of Technology, Pasadena, CA 91125.

[7] Physics Department, 366 LeConte Hall, University of California at Berkeley, Berkeley, CA 94720.

[8] Enrico Fermi Institute and Department of Physics, 933 E. 56th Street, University of Chicago, Chicago, IL 60637.

[9] Department of Physical Sciences, Eastern New Mexico University, Portales, NM 88130.

[10] Present address: Department of Physics, University of California, Santa Barbara, CA 93106.

The overabundance of negative electrons over positrons demonstrates that electrons consist of two populations: primary electrons accelerated in sources which may or may not be the same as the sources of hadronic cosmic rays, and secondary negative and positive electrons (in about equal proportions) that are produced subsequent to nuclear interactions in the interstellar medium (ISM). Primary contributions to the positron flux, if they exist, appear to be small. As indicated by radio observations, the most likely sources of primary electrons are supernova remnants (SNR), and recent X-ray and gamma-ray observations have identified one shell-type SNR (SN 1006) as a likely accelerator of electrons up to very high energy, around 100 TeV (Koyama et al. 1995; Tanimori et al. 1998).

Electrons are distinct from all other cosmic-ray particles by the absence of hadronic interactions, and, because of their low mass, by significant electromagnetic energy losses during propagation through the galaxy. The imprint of such energy losses on the energy spectrum of electrons permits interesting conclusions about the containment and source distribution of cosmic rays in the galaxy. We therefore briefly summarize the relevant facts.

At energies above a few GeV, energy losses due to synchrotron radiation in the galactic magnetic fields and inverse Compton scattering off photons (in particular the microwave background) are the dominant processes. These processes have an energy loss rate (dE/dt) whose magnitude increases with the square of the electron energy:

$$\frac{dE}{dt} = -kE^2, \text{ with } k = C\left(w_{\rm ph} + \frac{\langle B^2\rangle}{8\pi}\right). \quad (1)$$

The constant C equals 10^{-16} if the energy densities of photons and magnetic fields, $w_{\rm ph}$ and $\langle B^2\rangle/8\pi$, respectively, are measured in eV cm^{-3}, and dE/dt in GeV s^{-1}.

Consequently, the energy of an electron starting with energy E_0 decreases with time as $E(t) = E_0/(1 + kE_0\,t)$, and the "radiative lifetime" $\tau(E) = 1/kE$, is the time after which an electron starting with $E_0 \gg E$ has reached the energy E. This lifetime is too short to permit electrons to travel intergalactic distances through the cosmic microwave back-

ground; hence, electrons are the only cosmic-ray species for which an extragalactic contribution can be excluded with certainty.

For diffusive propagation of electrons inside the galaxy, with diffusion coefficient D, we can define a radiative propagation path length λ:

$$\lambda(E) = (2D\tau)^{1/2} \text{ if } D \text{ is constant, or}$$

$$\lambda(E) = \left(\int_E^\infty \frac{2D(E')dE'}{kE'^2} \right)^{1/2} \text{ if } D \text{ depends on energy .} \quad (2)$$

The observed intensity and energy spectrum of electrons is affected if λ becomes commensurate with the characteristic dimensions of the containment volume or with the scale of the spatial distribution of galactic sources. With the common assumption that all electron sources have a power-law source spectrum $E^{-\gamma_0}$ and are concentrated in the galactic disk, of scale size ("thickness") d, but that the containment volume includes a galactic halo of scale size h ($h \gg d$), one predicts several regions for the observed energy spectrum.

(a) Low energies, $\lambda(E) > h$.—The observed energy spectrum dn/dE, is determined by diffusive escape from the halo; radiative energy losses are insignificant. Thus, $dn/dE \propto D^{-1}E^{-\gamma_0}$. If D is independent of energy, the observed spectrum has the same slope as the source spectrum.

(b) High energies, $\lambda(E) < d$.—The propagation of electrons is dominated by radiative energy losses. In this energy region, electrons cannot escape from the galactic disk before losing most of their energy. Now we have $dn/dE \propto E^{-\gamma_0+1}$. The spectral index is exactly one unit larger than that of the source spectrum and independent of D. If E is very large, the discrete nature of sources in the disk becomes a limiting factor, and another scale length, ℓ; the average distance between sources becomes a limiting factor. One expects a sharp drop-off of the observed electron intensity if $\lambda < \ell$.

(c) Intermediate energies, $h > \lambda(E) > d$.—The containment volume depends on energy: electrons of initial energy, E_0, can only fill a volume of scale $\lambda(E_0)$. The observed energy spectrum will be steeper than the source spectrum but will also be affected by any energy dependence of D. An exact solution of the propagation equation for cylindrical symmetry by Dogiel & Sharov (1990) gives $dn/dE \propto D^{-1/2}E^{-(\gamma_0+0.5)}$.

Thus, one predicts a steepening of the observed spectrum over a characteristic range of energies. The spectral slope γ may vary from γ_0 to a maximum value $\gamma = \gamma_0 + 1$ (provided $\lambda > \ell$) if D is independent of energy, but the change in slope is smaller if D increases with energy. The value and the energy dependence of the diffusion coefficient are not well known but can, in principle, be determined from a precise measurement of the electron spectrum if this simple model is correct. Another unknown quantity is the source spectral index, γ_0. However, it should be noted that the "source spectrum" of positrons can be obtained from the spectra of primary nuclei if all positrons come from interstellar nuclear interactions.

Of course, there are more parameters that can, and perhaps must be, introduced. These include anisotropic diffusion, convection, and reacceleration in interstellar space. Others are solar modulation and bremsstrahlung losses at low energy, and Klein-Nishina corrections to the inverse Compton formula. But the more serious challenge is for the observer: one must obtain data on the electron spectrum which are accurate enough to permit a determination not only of the average spectral index γ, but also of its variation $\gamma(E)$ over a large range of energies. Only then will it be possible to derive robust constraints on the propagation process (DuVernois 1997).

In this paper, we shall present the results on the electron energy spectrum obtained with the HEAT experiment, and we shall discuss the data, together with results from other groups, in the context of a simple diffusion model. The primary purpose of HEAT was a measurement of cosmic-ray positrons, and results on the positron fraction have been reported previously (Barwick et al. 1995, 1997a). The instrument is also capable of measuring the absolute energy spectra of electrons and positrons separately, as well as the all-electron spectrum ($e^+ + e^-$). Results on these quantities, based on the first balloon flight of HEAT, were given by Barwick et al. (1998a). The present paper summarizes and discusses the total data set that has been accumulated in two flights in 1994 and 1995.

2. INSTRUMENT, BALLOON FLIGHTS, AND PERFORMANCE

The HEAT detector is described in detail elsewhere (Barwick et al. 1997b). It consists of a superconducting magnet and a drift-tube hodoscope (DTH) combined with a transition-radiation detector (TRD), an electromagnetic calorimeter (EC), and time-of-flight (TOF) scintillators. Figure 1 shows the cross section of the instrument. The instrument has a geometric acceptance of 495 ± 1 cm^2 sr. It was flown on balloons in 1994 and 1995. Although the basic set of detectors used in both flights remained the same, there are a few minor differences which affect overall performance. In the 1995 Lynn Lake flight, one of the six layers of the TRD was nonfunctional, as were a small number of drift tubes. The resulting slight losses of hadron rejection

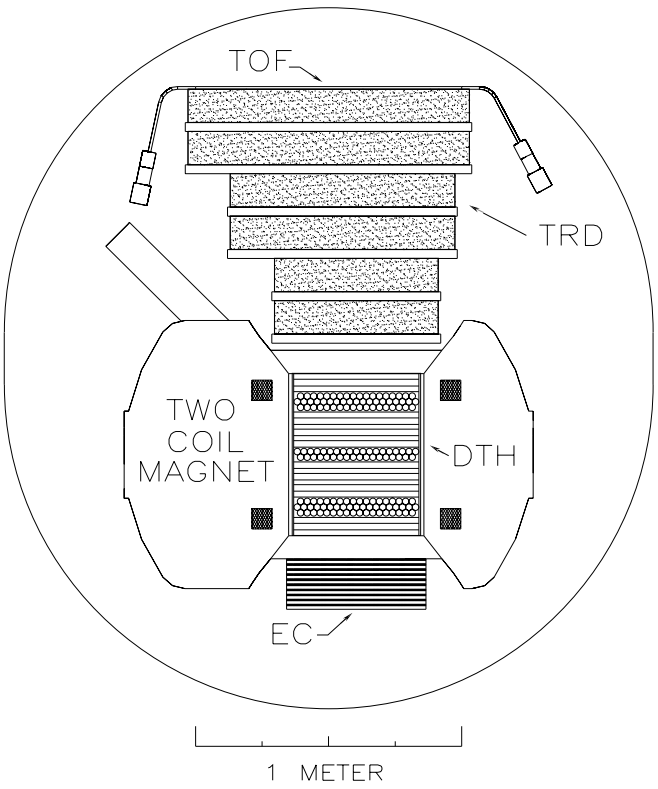

FIG. 1.—Schematic cross section of the HEAT instrument

power were compensated by using tighter electron selection criteria in the data analysis, thereby reducing electron efficiency.

The first balloon flight was on 1994 May 3–5 from Fort Sumner, NM. Data were collected at float altitude for about 29 hours, at a mean atmospheric overburden of 5.7 g cm^{-2}, and at vertical geomagnetic cutoff rigidities between 4 and 4.5 GV. The second flight was from Lynn Lake, Manitoba, on 1995 August 23–24. Data were collected for nearly 26 hours at a mean atmospheric overburden of 4.8 g cm^{-2} and a cutoff well below 1 GV.

Measurements of the positron fraction from both flights (Barwick et al. 1995, 1997a) and absolute differential energy spectra from the Fort Sumner flight (Barwick et al. 1998a) have been reported previously. Here we present the absolute energy spectra measured in the Lynn Lake flight, as well as the results combined for the two flights.

3. DATA ANALYSIS

The analysis approach has been described in more detail by Barwick et al. (1998a). Here we only summarize the procedures. The highest energy bin (50–100 GeV) is beyond the resolution limit of the magnet spectrometer, and only combined electron (electron plus positron) data are determined. Table 1 summarizes the criteria used in the analysis to select cosmic-ray events. Accepted electron and positron events must, in addition, be singly charged ($0.68 < |Z| < 1.45$), have showers that start early in the EC ($t < 0.89$ radiation length), have electron-like shower profiles ($\chi^2 < 2.6$), and be characterized by the evidence of transition radiation in the TRD (details of the TRD analysis are discussed by Barwick et al. 1998a). To determine the signature of interacting proton events that are most likely to masquerade as positrons, events are selected that satisfy all the above criteria except an absence of transition radiation.

TABLE 1

DATA CLEANLINESS SELECTION CRITERIA

DTH filter algorithm passed
DTH rigidity reconstruction algorithm passed
Number of tubes in DTH bending view used in fit ≥ 9[a]
Number of tubes in DTH bending view used in fit ≥ 8[b]
Number of tubes in DTH nonbending view used in fit ≥ 4
$\chi^2 < 10.0$ (DTH rigidity goodness of fit)[a]
$\chi^2 < 11.5$ (DTH rigidity goodness of fit)[b]
Average residual in X (nonbending) projection < 0.080 cm
Average residual in Y (bending) projection < 0.014 cm[a]
Average residual in Y (bending) projection < 0.030 cm[b]
Average residual in Z (vertical) projection < 0.020 cm
$\int B\,dl$ (Integrated B-field over the track length) > 2.2 kG m[c]
MDR > 60 GV[c]
MDR$/R > 4$[c]
$\lvert E/pc \rvert < 3.0$[a,c]
$\lvert E/pc \rvert < 4.0$[b,c]
$0.70 < \beta < 1.65$ (Velocity range, downward-going)
Agreement between DTH track and TOF timing < 20 cm
Propagated DTH track traverses both TOF and EC
Propagated DTH track traverses ≥ 4 TRD chambers

NOTE.—Except when indicated, selections are applied to both the HEAT-94 (Fort Sumner) and HEAT-95 (Lynn Lake) flight data.

[a] HEAT 1994 flight only.

[b] HEAT 1995 flight only.

[c] This selection is not used in the 50–100 GeV energy range.

A GEANT/FLUKA-based Monte Carlo (MC) simulation is employed to obtain efficiency-corrected geometrical factors and to model the atmospheric background from interacting protons, which is then subtracted from the electron and positron spectra. The electron energies are corrected for bremsstrahlung losses in the residual atmospheric overburden.

3.1. *Template Fits on Electrons and Interacting Protons*

The events selected as described above fall into two subsets: electrons ($e^{\pm}$) and interacting protons.

For these events, distributions of the ratio of the experimentally determined energy E (from the EC), and momentum p (from the DTH) are generated. For electrons and positrons, these distributions have a sharp peak at $E/pc = -1$ or $+1$, respectively. For interacting protons, the distribution peaks near $+0.5$, as a considerable fraction of the proton energy escapes from the EC. This difference in the shape of the distributions permits the identification of proton background remaining in the set of candidate positron events.

The measured E/pc distributions for negatively charged electrons are free of background and can be used directly to obtain templates for the expected E/pc distributions for both e^+ and e^-. As mentioned, the E/pc distributions for interacting protons are obtained by inverting the TRD selection for electrons. Both template distributions are smoothed and are used to fit the observed E/pc distribution for positron candidates. A Bayesian analysis is then used to estimate the number of electrons, positrons, and protons in each energy interval. The prior probability distributions are assumed to be flat for electrons, positrons, and protons, and they have conditional probability distributions taken from the template fits. The resulting numbers of positrons and electrons are indicated in Table 2 along with the 16% and 84% ("1 σ") Bayesian error limits. The energy bins used in Table 2 are energies at the top of the atmosphere, and the numbers of events are corrected for atmosphere secondary contributions as described below. The full details of this template analysis technique are described in Barwick et al. (1998a, 1998b).

Above 50 GeV, the selection criteria are loosened to gain statistics for the all-electron case. Without bending information being available at these energies, no electron-positron separation is possible. Templates and errors are, however, generated in the same way as for the lower energy bins.

TABLE 2

RAW NUMBERS OF ELECTRONS (1995 FLIGHT)

Energy (GeV)	Number of Electrons ΔN_{e^-}	Number of Positrons ΔN_{e^+}	Number of All-Electrons ΔN_e
1.0–1.5.....	1137 ± 34	241 ± 16	1378 ± 38
1.5–2.0.....	2157 ± 47	408 ± 21	2565 ± 52
2.0–3.0.....	3277 ± 58	423 ± 21	3700 ± 62
3.0–4.0	1959 ± 44	204 ± 15	2163 ± 47
4.0–5.0.....	1214 ± 35	114 ± 11	1328 ± 37
5.0–6.0	672 ± 26	62 ± 8	734 ± 27
6.0–8.9.....	884 ± 30	88 ± 10	972 ± 32
8.9–14.8	526 ± 23	45^{+8}_{-7}	571 ± 24
14.8–26.5	170 ± 13	$12.4^{+3.9}_{-3.3}$	182 ± 14
26.5–50.0	35^{+7}_{-6}	$2.7^{+1.9}_{-1.7}$	38^{+8}_{-7}
50.0–100.0.....			$9.4^{+3.7}_{-3.1}$

TABLE 3

ENERGY INTERVALS AND EFFECTIVE ACCEPTANCES

Energy (GeV)	$\bar{E}$ (GeV)	ΔE (GeV)	$\epsilon\Omega A$ (cm^2 sr)
1.0–1.5	1.20	0.50	108 ± 6
1.5–2.0	1.71	0.50	108 ± 6
2.0–3.0	2.40	0.99	110 ± 6
3.0–4.0	3.42	0.98	107 ± 6
4.0–5.0	4.44	0.98	107 ± 6
5.0–6.0	5.45	0.98	105 ± 6
6.0–8.9	7.16	2.78	111 ± 6
8.9–14.8	11.1	5.50	114 ± 7
14.8–26.5	18.9	10.7	112 ± 7
26.5–50.0	34.5	21.1	109 ± 6
50.0–100.0	66.4	44.0	116 ± 7

The same energy bins are used for the analysis of the two balloon flights. Mean energies for each bin and the effective bin widths in energy are calculated as described in § 4 and are summarized in Table 3.

3.2. *Monte Carlo Simulations*

Monte Carlo (MC) simulations are performed to determine the instrument response to primary particles, as well as the atmospheric production of secondary electrons and positrons. A code based on GEANT/FLUKA (Brun et al. 1994; ; Fassó et al. 1994) is used. The actual detector configurations for each flight (due to the minor differences in configuration) are separately modeled, as are the experimentally determined fluctuations in instrument response. The MC "events" simulate the flight data quite well, and the effects of the atmospheric simulation are also borne out in the data (for details, see Barwick et al. 1998a).

3.2.1. *Instrument Acceptance and Efficiency Corrections*

The instrument acceptance is calculated from the MC simulations as the product of the absolute efficiency ϵ and the geometrical aperture ΩA for electrons. The flight and MC event sets are subjected to similar sets of selection criteria and are compared directly when possible (see Barwick et al. 1998a). For example, the DTH electron selection efficiency is determined by taking electron events based on the EC, TOF, and TRD selections, and measuring the fraction of events which satisfy the DTH criteria. A visual scanning of several hundred flight and MC events indicated a small difference, on the order of 10% in selection efficiency, between simulated and experimentally measured events, which is taken into account in determining the overall instrumental acceptance.

TABLE 4

SECONDARY-TO-PRIMARY ELECTRON RATIOS AT 6 g cm^{-2}

Energy (GeV)	MC sec./pri.
1.0–1.5	0.14 ± 0.02
1.5–2.0	0.12 ± 0.02
2.0–3.0	0.08 ± 0.01
3.0–4.0	0.07 ± 0.01
4.0–5.0	0.07 ± 0.01
5.0–6.0	0.06 ± 0.01
6.0–8.9	0.06 ± 0.01
8.9–14.8	0.05 ± 0.01
14.8–25.6	0.05 ± 0.01
25.6–50.0	0.04 ± 0.02
50.0–100.0	0.03 ± 0.02

The calculated acceptances are shown in Table 3. The average electron acceptance efficiency is about 21% for the Lynn Lake flight, which is significantly lower than the value of 37% found for the first flight at Fort Sumner. This difference arises from reduced efficiency in the DTH due to failed drift tubes, worsened resolution, and excess random triggers during the second flight. The degradation of instrument response is believed to be related to moisture and condensation problems at Lynn Lake before the launch. The uncertainties in Table 3 are determined from adding the uncertainties of individual efficiency factors in quadrature.

It may happen than an event of some energy E, in a given energy bin, is reconstructed with an energy E' which falls into a different energy bin. This is accounted for on the basis of the MC simulations. Due to the steeply falling energy spectrum, about 2%–5% of MC events are reconstructed into the next higher energy bin, while about 20%–30% are reconstructed into the previous lower energy bin.

3.2.2. *Atmospheric Corrections*

The electron and positron spectra at balloon altitudes are composed of both primary incident particles and secondaries from interactions of incident cosmic rays in the atmosphere. (Reentrant albedo electrons are only important below local geomagnetic cutoff.)

The secondary flux in the atmosphere is estimated with a MC simulation using the FLUKA hadronic interaction algorithm (Fassó et al. 1994), assuming an incident proton spectrum with a power-law index of 2.74. The resulting secondary/primary electron ratios at 6 g cm^{-2} are shown in Table 4. As the atmospheric production of electrons is charge-sign independent, the fraction of positrons which are secondary ($\sim$30% at a few GeV) is higher than the secondary fraction of e^- ($\sim$3% at a few GeV). The uncertainties due to the atmospherics dominate the errors for the positron intensity at high energies and are significant at all energies.

The reliability of the secondary production calculation has been discussed by Barwick et al. (1998a, 1998b). The positron fraction as a function of atmospheric depth ("growth curve"), when extrapolated to the top of the atmosphere (ToA), agrees with the predictions of the MC atmospheric secondary production calculation.

4. RESULTS

The absolute differential energy spectra of the primary cosmic-ray electrons and positrons are obtained from the raw counts ΔN in Table 2 and the parameters from Tables 3 and 4 by calculating

$$j_{\rm pri}(\bar{E}) = \frac{f_{\rm ToA}\,\Delta N}{\Delta E \epsilon \Omega A \Delta t} - j_{\rm sec}(\bar{E})\,, \tag{3}$$

with

$$\bar{E} = \frac{\int_{E_i}^{E_j} E j_{\rm pri}(E) dE}{\int_{E_i}^{E_j} j_{\rm pri}(E) dE}\,, \tag{4}$$

and

$$\Delta E = \frac{\int_{E_i}^{E_j} j_{\rm pri}(E) dE}{j_{\rm pri}(\bar{E})}\,, \tag{5}$$

where an atmospheric secondary component is subtracted to obtain the primary component. Here $\epsilon\Omega A$ is the instrumental acceptance found from the MC calculations, Δt is the instrument live time, "pri" and "sec" stand for primary and secondary, respectively, E_i and E_j are the lower and upper bounds on each ToA energy interval, ΔE is the weighted average ToA energy interval, and $f_{\rm ToA}$ is a correction factor from the transformation (due to bremsstrahlung energy losses) of the measured energy to the energy at the top of the atmosphere (see Barwick et al. 1998a). In determining E and ΔE, an initial power-law ($E^{-\alpha}$) spectrum is assumed. This works well at high energy with α near 3.1 (Barwick et al. 1998a), but at lower energies the spectral shape changes to a lower effective α. This effective spectral shape, $\alpha_{\rm eff}$, is used at lower energies.

Table 5 shows the differential intensities $j_{\rm pri}(\bar{E})$ for electrons, positrons, and all-electrons ($e^+ + e^-$) taken from Barwick et al. (1998a) for the first flight (Fort Sumner), and Table 6 gives the results for the Lynn Lake 1995 flight.

Because of the essentially identical instrument configurations and analysis techniques for the two flights, combining the data is straightforward. The systematic errors in the two analyses, which arise primarily from the secondary corrections and the visual scanning, are essentially the same. Therefore, we can add the two data sets, weighted in each bin by their statistical significance, with statistical errors accounted for in the addition and systematic errors reintroduced to the combined data at the end.

Table 7 shows the resulting intensities for the combination of the Fort Sumner (1994) and Lynn Lake (1995) data sets. The electron and positron spectra are shown in Figure 2. The curve on the positron plot comes from a prediction for the interstellar spectrum by Moskalenko & Strong (1998), and the dashed line characterizes the arriving spectrum after applying a solar modulation correction to the Moskalenko & Strong spectrum. For comparison, Figure 2 also shows the results of other magnet spectrometer experiments (Buffington et al. 1975; Golden et al. 1996) for which absolute electron and positron intensities were reported.

Figure 3 shows the all-electron spectrum ($e^+ + e^-$). For comparison, we also show a recent result from another magnet spectrometer (Golden et al. 1996), and the recent data obtained with an imaging calorimeter (Torii et al. 1999). The agreement between these data sets is quite good, although at the highest energies our electron intensities

TABLE 5

DIFFERENTIAL INTENSITIES OF ELECTRONS AND POSITRONS AT THE TOP OF THE ATMOSPHERE, IN $(m^2\ s\ sr\ GeV)^{-1}$ FOR FORT SUMNER 1994 DATA

$\bar{E}$ (GeV)	$j^-_{\rm pri}(\bar{E})$	$j^+_{\rm pri}(\bar{E})$	$j^\pm_{\rm pri}(\bar{E})$
5.45	1.13 ± 0.12	0.076 ± 0.016	1.20 ± 0.13
7.16	0.548 ± 0.057	0.0405 ± 0.0070	0.589 ± 0.062
11.09...	0.141 ± 0.016	$(9.2^{+2.1}_{-2.0}) \times 10^{-3}$	0.151 ± 0.017
18.94...	0.0278 ± 0.0033	$(1.0^{+0.52}_{-0.38}) \times 10^{-3}$	0.0288 ± 0.0035
34.53...	$(3.64^{+0.62}_{-0.58}) \times 10^{-3}$	$(2.1^{+1.9}_{-1.1}) \times 10^{-4}$	$(3.84^{+0.64}_{-0.60}) \times 10^{-3}$
66.4			$(3.30^{+1.11}_{-0.83}) \times 10^{-4}$

NOTE.—Table taken from Barwick et al. 1998a.

TABLE 6

DIFFERENTIAL INTENSITIES OF ELECTRONS AND POSITRONS AT THE TOP OF THE ATMOSPHERE, IN $(m^2\ s\ sr\ GeV)^{-1}$ FOR LYNN LAKE 1995 DATA

$\bar{E}$ (GeV)	$j^-_{\rm pri}(\bar{E})$	$j^+_{\rm pri}(\bar{E})$	$j^\pm_{\rm pri}(\bar{E})$
1.20	3.19 ± 0.21	0.474 ± 0.057	3.66 ± 0.22
1.71	6.12 ± 0.38	0.820 ± 0.081	6.94 ± 0.39
2.40	4.71 ± 0.28	0.429 ± 0.041	5.14 ± 0.28
3.42	2.92 ± 0.18	0.206 ± 0.027	3.13 ± 0.18
4.44	1.81 ± 0.12	0.109 ± 0.019	1.92 ± 0.12
5.45	1.026 ± 0.073	0.065 ± 0.014	1.091 ± 0.074
7.16	0.449 ± 0.029	0.032 ± 0.006	0.481 ± 0.030
11.09.....	0.133 ± 0.010	$(8.2^{+2.2}_{-1.8}) \times 10^{-3}$	0.141 ± 0.011
18.94.....	0.0223 ± 0.0022	$(1.2^{+0.5}_{-0.4}) \times 10^{-3}$	0.0235 ± 0.0023
34.53.....	$(2.4^{+0.5}_{-0.4}) \times 10^{-3}$	$(1.4^{+1.4}_{-1.0}) \times 10^{-4}$	$(2.6^{+0.5}_{-0.4}) \times 10^{-3}$
66.4			$(3.1^{+1.6}_{-1.2}) \times 10^{-4}$

TABLE 7

DIFFERENTIAL INTENSITIES OF ELECTRONS AND POSITRONS AT THE TOP OF THE ATMOSPHERE, IN $(m^2\ s\ sr\ GeV)^{-1}$ FOR THE COMBINED FORT SUMNER 1994 AND LYNN LAKE 1995 DATA SET

$\bar{E}$ (GeV)	$j^-_{\rm pri}(\bar{E})$	$j^+_{\rm pri}(\bar{E})$	$j^\pm_{\rm pri}(\bar{E})$
1.20	3.19 ± 0.21	0.474 ± 0.057	3.66 ± 0.22
1.71	6.12 ± 0.38	0.820 ± 0.081	6.94 ± 0.39
2.40	4.71 ± 0.28	0.429 ± 0.041	5.14 ± 0.28
3.42	2.92 ± 0.18	0.206 ± 0.027	3.13 ± 0.18
4.44	1.81 ± 0.12	0.109 ± 0.019	1.92 ± 0.12
5.45	1.095 ± 0.058	0.072 ± 0.012	1.167 ± 0.061
7.16	0.514 ± 0.026	0.038 ± 0.006	0.552 ± 0.027
11.09.....	0.138 ± 0.008	$(8.9^{+1.7}_{-1.5}) \times 10^{-3}$	0.147 ± 0.008
18.94.....	0.0259 ± 0.0020	$(1.1^{+0.5}_{-0.4}) \times 10^{-3}$	0.0270 ± 0.0021
34.53.....	$(3.2^{+0.5}_{-0.4}) \times 10^{-3}$	$(1.9^{+1.4}_{-1.0}) \times 10^{-4}$	$(3.4^{+0.6}_{-0.5}) \times 10^{-3}$
66.4			$(3.2^{+1.0}_{-0.8}) \times 10^{-4}$

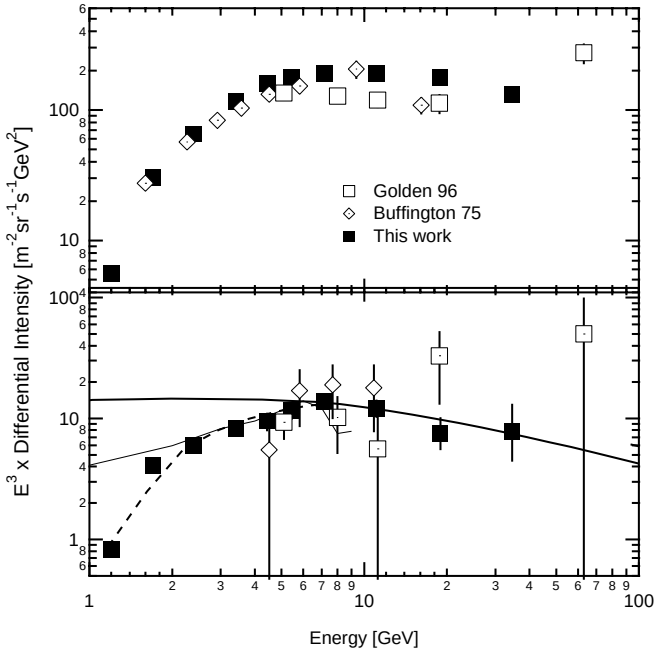

FIG. 2.—Absolute differential energy spectra for electrons (*top*) and positrons (*bottom*), multiplied by E^3, for the combined 1994 and 1995 data set; the solid line is a prediction from Moskalenko & Strong (1998) without solar modulation; the dashed line is a solar-modulated version of the Moskalenko & Strong (1998) results.

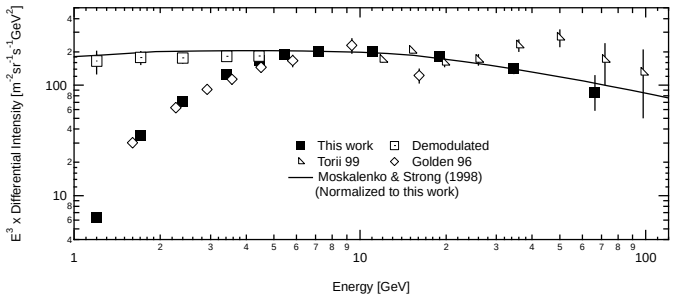

FIG. 3.—Absolute differential energy spectrum for all electrons $(e^+ + e^-)$ for the combined 1994 and 1995 data set. Two other recent measurements are shown for comparison. The open squares at low energies are obtained when the HEAT data are demodulated to local interstellar space (see text), and the solid line refers to a calculated prediction.

seem to be slightly lower than those reported by Torii et al. (1999). The solid line again gives the predicted shape of the interstellar energy spectrum according to Moskalenko & Strong. The open squares at low energy are derived after applying a demodulation correction to our data with the same modulation parameters as in Figure 2. In this demodulation, we use the numerical treatment of Fisk (1971) as refined by Moraal (1976) and Beatty et al. (1993). In the force-field approximation, the modulation parameters are 755 and 670 MV for the 1994 and 1995 data sets, respectively. In Figure 4, we plot the positron fraction $e^+/(e^+ + e^-)$ as a function of energy for the combined data set of the two HEAT flights and include the results of other experiments for comparison. The data shown in this figure have already been reported (Barwick et al. 1997a).

5. DISCUSSION

The results obtained with the HEAT magnet spectrometer are characterized by a high level of hadronic background rejection. A comparison of our data with those of other groups reveals the following.

5.1. *Individual Spectra of Electrons and Positrons*

As Figure 2 indicates, there is good agreement on the spectrum of negative electrons between three different magnet spectrometer observations. For positrons, the agreement with other measurements is not so obvious, but large statistical uncertainties in some of the data preclude a quantitative comparison. We notice that the spectrum of positrons appears to decrease a little less sharply toward low energy than that of negative electrons. The prediction by Moskalenko & Strong (1998) is made under the assumption that all positrons are generated in the decay of particles (mostly pions) produced in nuclear cosmic-ray interactions in the ISM. Their model depends on knowledge of the absolute proton intensity in the Galaxy, and on assumptions on propagation through the Galaxy, however, as shown in Figure 2, the model agrees quite well with the positron intensity measured by HEAT. Thus, on the basis of this comparison, we see no significant indication for a contribution to the measured intensity of positrons other than that from interstellar secondary production.

5.2. *Positron Fraction*

As reported earlier (Barwick et al. 1997a), the positron fraction, shown in Figure 4, does not exhibit the increase above 10 GeV that was reported in some earlier measurements (Agrinier et al. 1969; Müller & Tang, 1987; Golden et al. 1987). This again seems to rule against a significant excess of primary positrons of unknown origin in this region. However, a slight irregularity in the spectral shape around 7 GeV cannot be excluded. The significance of such a "feature" and its possible origin have been discussed in a separate paper (Coutu et al. 1999).

5.3. *All-Electron Spectrum*

When we compare the all-electron spectrum measured with HEAT with earlier data, we find significant discrepancies in the overall data set. This is illustrated in Figure 5, where we plot the all-electron spectrum data published since 1975. The absolute flux values vary by a factor of about 2 in the region around 10 GeV where the counting statistics are generally quite good. Due to these differences, the overall slope of the energy spectrum cannot be determined with great accuracy.

The results reported here, along with those of the two most recent observations of other groups (see Fig. 5), tend to lie on the low side of the reported intensities. Our spectrum, if extrapolated to higher energies, would significantly undershoot the measurement of Kobayashi et al. (1999) which is the only measurement reporting results above ~ 300 GeV. The differences between the individual data sets could result either from undetected hadronic background (at least in those data that report high fluxes), from systematic uncertainties in the energy scale (which are amplified if the flux values are multiplied by E^3), or from incorrect assessments of the overall instrumental acceptance effi-

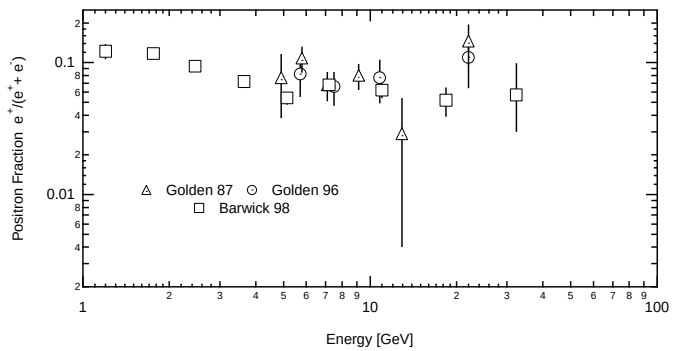

FIG. 4.—HEAT (Barwick et al. 1998a, 1998b) and other recent measurements of the positron fraction.

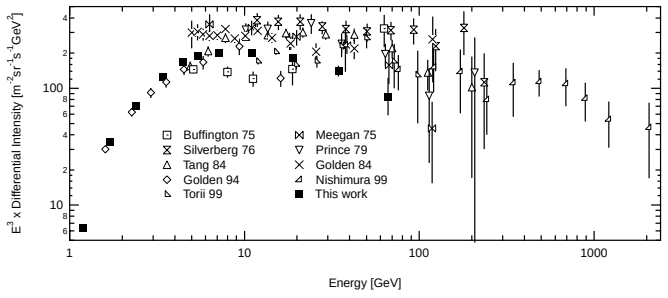

FIG. 5.—Absolute differential energy spectrum for all electrons $(e^+ + e^-)$ as measured by HEAT. A compilation of measurements since 1975 is included for comparison. [*See the electronic edition of the Journal for a color version of this figure.*]

ciencies. It is probably fair to assume that hadron contamination is not a major problem for measurements that use two independent techniques for hadron rejection, such as shower counters combined with magnet spectrometers or transition radiation detectors, or both. Acceptance efficiencies, on the other hand, are notoriously difficult to determine, but their assessment is probably more reliable in the recent observations, for which more powerful computer simulations could be made than in earlier investigations. If a measurement is in error either in the energy scale or in the acceptance efficiency by a constant (i.e., not energy-dependent) factor, then the power-law slope of the spectrum will not be affected. Assuming that this is the case, we may assess the overall power-law slope resulting from the entire data set of Figure 5 by arbitrarily normalizing the data to the same intensity at a given energy. This is done in Figure 6, using energies around 10 GeV for normalization. A least-squares fit to the spectra of Figure 6 to a single power-law spectrum above 20 GeV yields a spectral index of 3.30 ± 0.06.

It is interesting to discuss these results in the context of the diffusive propagation model reviewed above. First, let us assume that a power-law shape with index $\gamma = 3.30$ indeed characterizes the fully steepened spectrum [see § 1, energy region (b)]. This assumption is by no means certain, as a more complex spectral structure could be hidden by the uncertainties in the data. Nevertheless, under this assumption the spectrum of electrons *series at the sources* would have a power-law index $\gamma_0 = \gamma - 1 = 2.3$. This value is quite close to the power-law index deduced cosmic-ray nuclei at their sources, $\gamma_0 = 2.2 \pm 0.5$ (Müller et al. 1991; Swordy et al. 1993). Thus, if this interpretation is correct, one would conclude that electrons and nuclei are accelerated with the same source spectrum, and hence, most likely by the same sources.

At low energies, below 5 GeV, the asymptotic slope of the demodulated local electron spectrum (see Fig. 6) would have a power-law index of about $\gamma = 2.85$. Hence, the total change in power-law index from low to high energy is $\Delta\gamma \approx 0.5$. While one might be tempted to attribute this spectral change to a transition from region (b) to region (c) in the model described in § 1, this would require that the diffusion coefficient, D, is essentially independent of energy. Thus, the data reconfirm a fact that has already been recognized by Tang (1984): the change in slope of the electron spectrum is too rapid as to be easily compatible with energy-dependent diffusion *and* a source spectrum described by a single power law. Measurements of the nuclear cosmic-ray composition—in particular, measurements of the energy dependence of the relative abundance of secondary cosmic rays (e.g., the L/M ratio)—imply that the diffusion constant increases with energy. We are then led to the conclusion that the source spectrum of electrons cannot be characterized by a single power law over the entire energy range, but must become harder at lower energies.

A quantitative description of the propagation of electrons at low energies must include energy losses due to ionization and bremsstrahlung. An extensive computer simulation including these effects has been provided by Moskalenko & Strong (1998). These authors also conclude that their model can describe the measured data only if the electron source spectrum changes shape, with an index of 2.1 below 10 GeV, steepening to 2.4 above 10 GeV. This model uses either diffusion coefficients that are constant up to rigidities of 3 GV, and which then vary with rigidity as $\propto R^{0.6}$, or diffusion coefficients $\propto R^{0.33}$ for all rigidities but then also requiring reacceleration during propagation. A flattening of the electron source spectrum below 2 GeV was also inferred previously by Müller & Tang (1983), from an analysis of the nonthermal galactic radio background.

In principle, more detail on the propagation of electrons can be derived from separate observations of the energy spectra of negative electrons and positrons. As virtually all positrons appear to arise from interstellar nuclear interactions of cosmic-ray nuclei, their "source spectrum" can be calculated from the spectrum of primary nuclei; thus, one of the uncertain parameters in interpreting the measured data is removed. Unfortunately, the statistical accuracy of the data (see Fig. 2) does not yet permit strong conclusions. It must be noted, however, that the model of Strong and Moskalenko is in very good agreement with the HEAT positron measurement.

While not the subject of the HEAT data reported here, let us briefly comment on the highest energies, around 1000 GeV and beyond. It has been frequently pointed out by Nishimura and collaborators (e.g., Kobayashi et al. 1999)

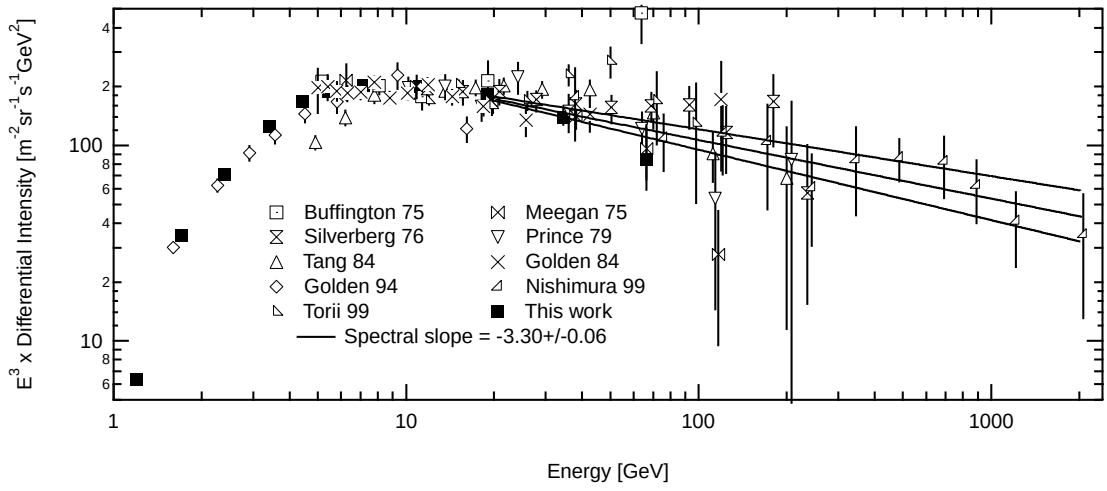

FIG. 6.—Absolute differential energy spectrum for all electrons as in Fig. 5. However, each reported intensity (except for the high-energy Kobayashi et al. 1999 measurement) is normalized to the HEAT results around 10 GeV. [*See the electronic edition of the Journal for a color version of this figure.*]

that for such energies, the electron path length becomes smaller than the dimensions of the galactic disk. Thus, the spatial distribution of galactic sources becomes important, and a sharp drop-off of the electron intensity is expected when λ becomes smaller than the distance to the nearest source. Kobayashi et al. argue that Vela, at a distance of 0.2–0.4 kpc, might be the nearest and perhaps only supernova remnant that could generate electrons in the TeV region. To prove this suggestion, new observations over an extended energy range and with improved statistics are clearly needed.

6. CONCLUSION

In spite of the efforts of many groups over the years, the interpretation of the electron data still remains somewhat tenuous. It appears that the source energy spectrum of electrons above $\sim$ 10 GeV has the same shape as that inferred for cosmic-ray nuclei. This would support a common origin of both particle species, most likely in supernova remnants. The source spectrum may not have a continuous power-law shape but may become somewhat harder below 10 GeV. The measured data constrain the value of the diffusion coefficient for interstellar propagation if the energy dependence of the diffusion is understood. In the context of the model described in § 1, and assuming that the energy spectrum reaches its fully steepened shape at a characteristic energy of 30 GeV, we obtain $D_0 = 7.5 \times 10^{26}$ cm^2 s^{-1} for $D = D_0(E/1\ \mathrm{GeV})^{0.6}$. (We use here canonical assumptions about the Galactic disk: $\alpha = 1$ kpc and $W_{\mathrm{ph}} + \langle B^2 \rangle / 8\pi = 1$ eV cm^{-3}.) Positrons are predominantly of interstellar secondary origin; possible unusual or cosmological contributions many still be hidden within the experimental uncertainties.

There are several key experiments that could help resolve the remaining questions. First, a new measurement with a single detector of proven capability to reject proton background that could cover the entire energy range from around 1 GeV to several TeV with good statistical accuracy, would be desirable. This is a difficult task, but may become feasible with the evolving capabilities of ultralong-duration balloons. In addition, nonstandard techniques should be explored to obtain measurements in the TeV region. These include observations of electrons via their emission of hard X-ray synchrotron radiation in the Earth's magnetic field (Stephens & Balahsubrahmanian 1983), or perhaps ground-based observations with Cherenkov telescope arrays such as VERITAS or HESS. Second, the accurate measurement of the positron spectrum, up to energies of a few hundred GeV, is necessary to better understand the propagation process and to further search for primary positron contributions. Again, this will require long-duration balloon flights or observations in space. Finally, to determine the energy dependence of diffusion, the propagation path length for cosmic rays must be studied with nuclear composition measurements extending far beyond the present limit of $\sim$100 GeV/n for the L/M ratio.

We gratefully acknowledge assistance from D. Bonasera, E. Drag, W. Johnson, P. Koehn, D. Kouba, R. Northrop, and J. Robbins. We also thank the NSBF crews that have supported the balloon flights. This work was supported by NASA grants NAG5-5059, NAG5-5069, NAG5-5070, NAGW-1035, NAGW-1995, NAGW-2000, and NAGW-4737, and by financial assistance from our individual institutions.

REFERENCES

Agrinier, B., et al. 1969, Nuovo Cimento Lett., 1, 53
Barbiellini, G., et al. 1996, A&A, 309, L15
Barwick, S. W., et al. 1995, Phys. Rev. Lett., 75, 390
Barwick, S. W., et al. 1997a, ApJ, 482, L191
Barwick, S. W., et al. 1997b, Nucl. Instrum. Methods Phys. Res., 400, 34
Barwick, S. W., et al. 1998a, ApJ, 498, 779
Barwick, S. W., et al. 1998b, J. Geophys. Res., 103, 4817
Beatty, J. J., et al. 1993, ApJ, 413, 268
Brun, R., et al. 1994, GEANT, Detector Description and Simulation Tool, V. 3.21, CERN Program Libraries (unpublished)
Buffington, A., Orth, C. D., & Smoot, G. F. 1975, ApJ, 199, 669
Coutu, S., et al. 1999, Astropart. Phys., 11, 427
Dogiel, V. A., & Sharov, G. S. 1990, A&A, 229, 259
DuVernois, M. A. 1997, ApJ, 481, 241
Fanselow, J. L., Hartman, R. C., Hildebrand, R. H., & Meyer, P. 1969, ApJ, 158, 771
Fassó, A., Ferrari, A., Ranft, J., & Sala, P. R. 1994, in Proc. Fourth Int. Conf. on Calorimetry in High Energy Physics, ed. A. Menzione & A. Scribano (Singapore: World Scientific), 20
Fisk, L. A. 1971, J. Geophys. Res., 76, 221
Golden, R. L., et al. 1984, ApJ, 287, 622
Golden, R. L., et al. 1987, A&A, 188, 145
Golden, R. L., et al. 1996, ApJ, 457, L103
Kobayashi et al. 1999, Proc. 26th Int. Cosmic-Ray Conf. (Salt Lake City), 61
Koyama, K., et al. 1995, Nature, 378, 255
Moraal, H. 1976, Space Sci. Rev., 19, 845
Moskalenko, I. V., & Strong, A. W. 1998, ApJ, 493, 694
Müller, D., & Tang, K. 1987, ApJ, 312, 183
Müller, D., et al. 1991, ApJ, 374, 356
Nishimura, J., et al. 1980, ApJ, 238, 394
Prince, T. A. 1979, ApJ, 227, 676
Stephens, S. A., & Balahsubrahmanian, V. K. 1983, J. Geophys. Res., 88, 7811
Swordy, S., et al. 1993, ApJ, 403, 658
Tang, K. K. 1984, ApJ, 278, 881
Tanimori, T., et al. 1998, ApJ, 497L, 25
Torii, S., et al. 1999, Proc. 26th Int. Cosmic-Ray Conf. (Salt Lake City), 53